International Journal of Heat and Mass Transfer 52 (2009) 3778–3789

Contents lists available at ScienceDirect

International Journal of Heat and Mass Transfer

journal homepage: www.elsevier.com/locate/ijhmt

Heat transfer enhancement by flow bifurcations in asymmetric wavy wall channels

Amador M. Guzmán *, Maria J. Cárdenas, Felipe A. Urzúa, Pablo E. Araya

Departamento de Ingeniería Mecánica, Universidad de Santiago de Chile, Alameda 3363, Estación Central, Santiago, Chile

ARTICLE INFO

Article history:
Received 10 June 2008
Received in revised form 19 February 2009
Accepted 19 February 2009
Available online 17 April 2009

Keywords:
Heat transfer enhancement
Asymmetric wavy wall channels
Flow bifurcations

ABSTRACT

The enhancement characteristics of heat transfer, through a transition scenario of flow bifurcations, in asymmetric wavy wall channels, are investigated by direct numerical simulations of the mass, momentum and energy equations, using the spectral element method. The heat transfer characteristics, flow bifurcation and transition scenarios are determined by increasing the Reynolds numbers for three geometrical aspect ratios $r = 0.25$, 0.375, and 0.5, and Prandtl numbers 1.0 and 9.4. The transition scenarios to transitional flow regimes depend on the aspect ratio. For the aspect ratios $r = 0.25$ and 0.5, the transition scenario is characterized by one Hopf flow bifurcation. For the aspect ratio $r = 0.375$, the transition scenario is characterized by a first Hopf flow bifurcation from a laminar to a periodic flow, and a second Hopf flow bifurcation from a periodic to quasi-periodic flow. The periodic and quasi-periodic flows are characterized by fundamental frequencies ω_1, and ω_1 and ω_2, respectively. For all the aspect ratios and Prandtl numbers, the time-average mean Nusselt number and heat transfer enhancement increases with the Reynolds number as the flow evolves from a laminar to a transitional regime. For both Prandtl numbers, the highest increase in the Nusselt number occurs for the aspect ratio $r = 0.5$; whereas, the lowest increases happen to $r = 0.25$. The increase of the Nusselt number occurs at the expense of a higher pumping power, which, for both Prandtl numbers, grows as the aspect ratio increases from $r = 0.25$ to $r = 0.5$ for reaching a specific Nusselt number. This enhancement is obtained without the necessity of high volumetric flow rates associated with turbulent flow regimes, which demand much higher pumping powers. Significant heat transfer enhancements are obtained when the asymmetric wavy channel is operated in the appropriate transitional Reynolds number range.

1. Introduction

An extensive amount of research has been performed in the last decades to obtain a better understanding of flow mixing and heat transfer enhancement in channels with geometrical inhomogeneities, such as asymmetric and symmetric wavy walls, grooved, communicating, and corrugated channels, as well as in other geometrical configurations, such as backward facing steps, channel expansions, passages with eddy promoters, and grooved tubes [1–14,17,18,23]. Asymmetric and symmetric wavy wall channels are used in industrial and biomedical applications, such as compact heat exchangers, oxygenators and hemo-dialyzers. Active and passive heat transfer enhancement techniques have been developed and investigated in an effort to enhance heat transfer processes by affecting the flow characteristics. Considerable efforts have been dedicated to the role of flow destabilization and flow mixing in heat transfer enhancement. Active flow modulation for example, has shown to be effective in producing resonant heat transfer enhancement. Investigations performed with wavy, grooved and communicating channels have demonstrated that self-sustained oscillations that develop in these geometries by exciting flow instabilities, lead to heat transfer enhancement without applying active forcing. It has been found that the enhancement of heat transfer varies, depending on specific geometric characteristics and boundary conditions.

Asymmetric and symmetric wavy channels have been considered in several earlier investigations to enhance heat and mass transfer rates in compact exchange devices such as heat exchanger and oxygenators. These channels are easy to fabricate and can provide significant heat transfer enhancement if operated in an appropriate Reynolds number range [15–21]. Early investigations have found no significant heat transfer enhancement for a steady laminar flow. However, if/when the flow becomes time-dependent – either through external forcing or natural self-sustained conditions –significant heat exchange enhancement can be obtained. Several investigations have found that a natural transition to a time-dependent periodic self-sustained flow regime leads to enhancement of heat transfer rates, with moderate and reasonable pressure drops. Guzmán and Amon [15–17] performed numerical investigations for high transitional Reynolds numbers in converging-diverging (symmetric wavy wall) channels and found that the flow develops a second bifurcation in addition to the first flow bifurcation at a Reynolds number $Rec_2 > Rec_1$, which enhances the flow

* Corresponding author. Tel.: +562 718 3104; fax: +562 682 3020.
E-mail address: amador.guzman@usach.cl (A.M. Guzmán).

0017-9310/$ - see front matter © 2009 Elsevier Ltd. All rights reserved.
doi:10.1016/j.ijheatmasstransfer.2009.02.026

Nomenclature

A	area
H	separation between walls
L	streamwise separation among furrows, periodic length
P	pressure
Q	volumetric flow rate
T	temperature, time period
Pe	Peclet number
Pr	Prandtl number
Re	Reynolds number
Rec	critical Reynolds number
Re_H	height based Reynolds number
k	thermal conductivity
n, m	integer numbers
$\overline{Nu}$	time-averaged mean Nusselt number, Nusselt number
$\overline{Nu}(t)$	time-dependent mean Nusselt number
$Nu(x,t)$	local Nusselt number
$q(x,t)$	local heat flux
$T_w(x,t)$	local lower wall temperature
T_b	bulk temperature
ΔP	pressure drop
$\hat{U}$	time-average mean streamwise velocity
$\vec{V}$	velocity
c_p	specific heat
dp/dx	pressure gradient
$\hat{h}$	half height of the channel
f_b	asymmetric wavy channel friction factor
f_p	plane channel friction factor

Greek symbols

α	thermal diffusivity
Φ	pumping power
μ	dynamic viscosity
ν	kinematic viscosity
ρ	density
ω	fundamental (critical) frequency

mixing and heat transfer process. Further numerical studies have indicated that a geometrical parameter (namely the aspect ratio $r = a/(2L)$), plays a role in both the type of transition scenario and the heat transfer enhancement characteristics. Experimental or numerical investigations of transition scenarios and heat transfer enhancement for higher transitional (but not turbulent), Reynolds numbers flow regimes for asymmetric wavy channels, have thus far not been reported.

This article describes numerical investigations of heat transfer enhancement due to flow bifurcations in asymmetric wavy channels in transition scenarios from laminar to transitional time-dependent flow regimes. Two-dimensional direct numerical simulations (DNS), of the time-dependent, incompressible continuity, Navier–Stokes, and energy equations are carried out for three (3) aspect ratios and two (2) Prandtl numbers. First, the flow evolution from a laminar to a transitional state through flow bifurcations is described by examining the velocity field, Fourier power spectra and pseudo-phase space representations; then, flow and heat transfer characteristics and parameters are determined through the transitional regime for increasing Reynolds numbers. Last, heat transfer enhancement comparisons are performed among the aspect ratios and related to the flow characteristics of the transition scenarios.

2. Problem definition, formulation, and numerical approach

The physical configuration of the asymmetric wavy channel used in this investigation (which contains 12 furrows), is shown in Fig. 1(a). The separation between the parallel asymmetric walls is $H = 2\hat{h} = 4.3333$, the distance between furrows is $L = 4.6666$; the amplitude of the sinusoidal wall is a, and the channel aspect ratio is $r = a/(2L)$. Fig. 1(b) shows one furrow of the channel with a spatial periodic length L. This investigation uses extended and reduced computational domains to: (a) demonstrate and verify the existence of a fully developed flow and self-similar temperature profiles; and, (b) investigate in detail the flow pattern and heat transfer enhancement characteristics and parameters for laminar and transitional regimes.

An incompressible and time-dependent flow of a Newtonian fluid for both the extended and reduced domains is considered. The flow is governed by the continuity and Navier–Stokes Eqs. (1) and (2); whereas, the heat transfer process is described by the energy Eq. (3). For the extended domain, a uniform velocity profile at the entrance of the channel, non-slip for upper and lower walls, and outflow for the channel exit, are imposed. For the heat transfer process, constant temperature at the entrance, vanishing heat flux on the upper wall, outflow for the exit, and constant heat flux in the lower wall, are imposed. For the one furrow reduced domain, spatial periodicity in the streamwise direction, which corresponds to a fully developed flow, is considered. In any equilibrium state, the resulting velocity profile at the domain inlet and outlet is the same, regardless of the laminar or transitional nature of the flow regime. For the heat transfer process, vanishing and constant heat fluxes are imposed on the channel upper and lower walls, respectively, and a self-similar temperature profile is imposed by enforcing spatial periodicity for the temperature in the streamwise direction. By imposing this mathematical spatial periodicity for the channel inlet and outlet, the temperature field obtained within the domain takes into account the contribution of the imposed heat flux on the lower wall to the increase of the flow temperature that enters into the domain. Thus, the outlet temperature is equal to the

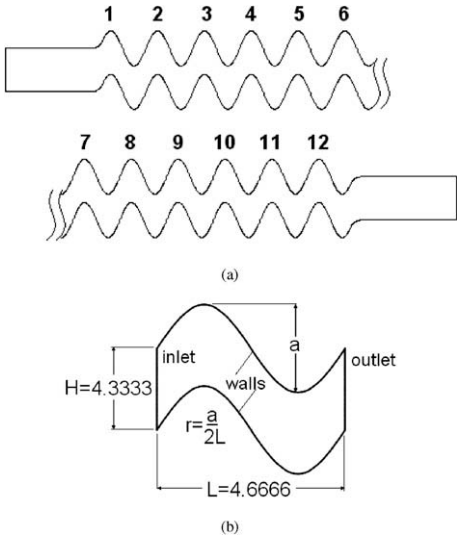

Fig. 1. Schematic of the asymmetric wavy wall channel: (a) extended domain with 12 furrows, plane inlet and outlet regions; (b) reduced periodic computational domain with spatially periodic length $L = 4.6666$, distance between walls $2\hat{h} = 4.3333$; and aspect ratio $r = a/(2L)$.

inlet temperature, plus the temperature rise caused by the incoming heat flux. In addition, the flow temperature at any given location between the inlet and outlet within the domain, rises with respect to the inlet temperature for the exact amount of heat received between the inlet and the given position. So, strictly speaking, the outlet and inlet temperatures are never equal, but their profiles are similar.

$$\nabla \cdot \vec{V} = 0 \tag{1}$$

$$\rho\left(\frac{\partial V}{\partial t} + \vec{V}\cdot\nabla\vec{V}\right) = -\nabla P + \mu\nabla^2\vec{V} \tag{2}$$

$$\rho c_p\left(\frac{\partial T}{\partial t} + \vec{V}\cdot\nabla T\right) = k\nabla^2 T \tag{3}$$

The governing equations are solved using a computational program based on the spectral element method (SEM). This method combines the high accuracy of the spectral methods with the geometric flexibility of the Finite Element Method [2,22]. The computational domains are discretized with macroelements that contain nodal points where velocity, pressure and temperature are represented. A mesh refinement study with different discretizations and mesh resolutions for the three aspect ratios is performed to establish the adequacy of the computational discretization and the imposed boundary conditions. Each aspect ratio requires a specific domain discretization.

Different computational meshes are used for the extended and reduced computational domains, with an increasing number of macroelements and nodal points, until acceptable, independent mesh results are achieved. The criteria used in this investigation is that the relative error for any given field variable – such as pressure, velocity and temperature between two consecutive meshes – is less than 0.1%. Fig. 2(a–c) show computational meshes for the extended and reduced domains, respectively, for the aspect ratio $r = 0.375$. Fig. 2(a) shows a computational mesh with 155 and 4 macroelements in the streamwise and crosswise directions, respectively, with 8×8 nodal points per macroelement, and 31494 nodes. A sufficiently long plane channel, and constant cross sections, is considered before the first furrow and after the last furrow, to obtain adequate representations of the boundary conditions. Fig. 2(b) and (c) show two computational meshes for the periodic reduced domain, with 16×4 and 16×8 macroelements, and 3741 and 7353 nodes, respectively. A regular discretization, in terms of macroelements in both the streamwise and crosswise directions, is used with a higher density of nodal points near the walls, where important velocity and temperature gradients are expected during transitional time-dependent flow regimes. Comparisons with available experimental and numerical simulations data, using an extended domain, are performed to verify and validate the spatial periodicity assumptions for flow and temperature (Nishimura [21], Vyas et al. [29], Stephanoff et al. [30], Nishimura and Matsune [31]). Most of the experimental data for asymmetric wavy channels have been obtained using either steady or pulsatile flows. Experimental visualizations of steady and pulsatile flows in a symmetric wavy channel with an aspect ratio $r = 0.125$, performed by Stephanoff et al. [30], demonstrated the existence of spatial periodicity in steady flow. Experimental visualizations, and numerical simulations of steady and externally pulsatile flows in symmetric and asymmetric wavy channels, performed by Nishimura [21], and Nishimura and Matsune [31], confirmed the spatial periodic nature of the flow. Photographs of flow visualizations clearly show the spatial periodicity in the channel central furrows. Recently, Vyas et al. [29] reported experimental and numerical simulation results of flow pattern and heat transfer characteristics in an asymmetric wavy channel with an aspect ratio $r = 0.125$, for a steady flow that agrees well with previously reported experimental and numerical results.

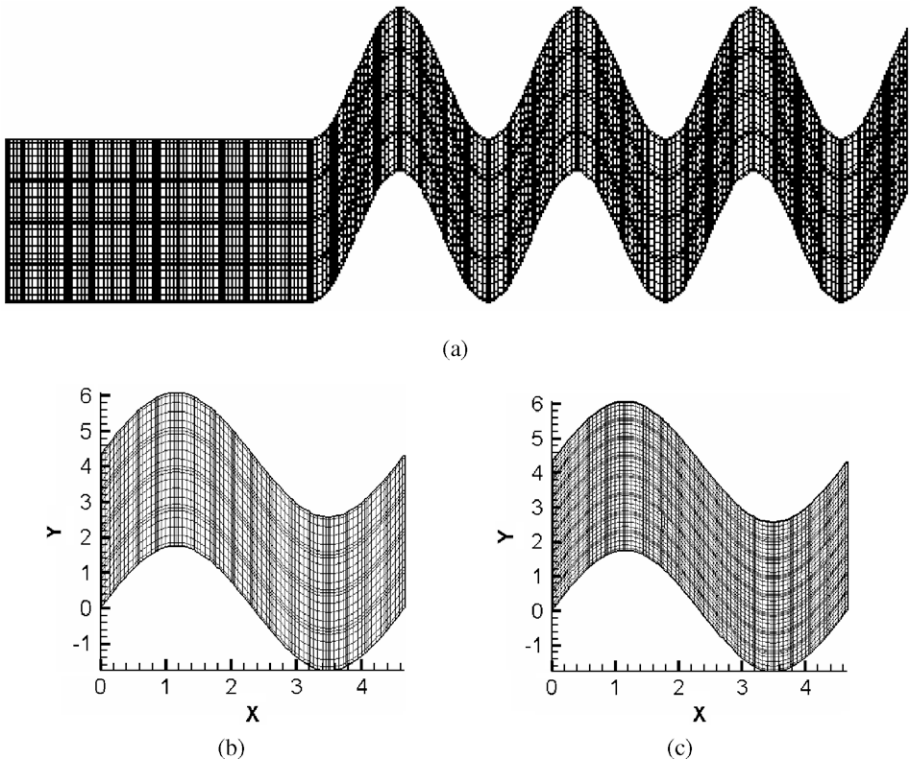

Fig. 2. Domain discretization for aspect ratio $r = 0.375$: (a) extended domain with entrance region and furrow discretizations; and, (b) reduced domain with two discretizations for one periodic length L. Total number of nodes for extended domain is 31494; whereas reduced domain has 3784 and 7353 nodes for (b) and (c) meshes, respectively.

Numerical simulations are performed for increasing Reynolds numbers in the laminar and transitional flow regime. The procedure for obtaining asymptotic stable states for a given Reynolds number consists of integrating, in time, the governing equations, starting with a predicted steady flow and gradually increasing the Reynolds number until a steady, time-periodic or quasi-periodic transitional state is found. Once an asymptotic stable state is obtained, the governing equations for a different Reynolds number are solved using the previous asymptotic state as the initial condition. For this investigation, the Reynolds number is defined as $Re = \frac{3}{2}\frac{\hat{U}\cdot\hat{h}}{\nu}$ where $\hat{U}$ is the time-average, mean streamwise velocity at the inlet of the channel – which is calculated as Q/A – with Q and A, the volumetric flow rate and the cross-sectional area, respectively; $\hat{h}$ is half the height of the channel at the inlet, and ν is the kinematic viscosity. The Prandtl number is defined as $Pr = \nu/\alpha$ where α is the thermal diffusivity. Since the fluid motion is induced by an external applied pressure drop, and not by body forces, the resulting flow pattern and characteristics are independent of the imposed thermal boundary conditions and temperature distribution. Flow and heat transfer simulations are performed for the aspect ratio $r = 0.25$, 0.375, and 0.5, Prandtl number $Pr = 1$ and 9.4, and for a Reynolds number range that corresponds to laminar and transitional flow regimes.

Fig. 3 shows the streamwise u-velocity as function of time of a typical point of the reduced domain. After an initial transient behavior, the flow evolves to a time-dependent periodic state. The evolution from a first state (not shown here), to the second (the periodic state), originates with an increase in the volumetric flow rate. In some cases this higher Reynolds flow regime was used as the initial condition for running a simulation with a lower volumetric flow rate (the previous initial state), the objective being to determine the existence of any possible hysteretic effects, which are important for determining the right bifurcation diagram. So far, no hysteretic effects were detected for the aspect ratios of this investigation in the range of the laminar and transitional flow simulations.

3. Numerical results and discussion

3.1. Flow regimes for an extended domain

Numerical investigations of spatial periodicity for both laminar and transitional flow regimes are performed for the three aspect ratios of this asymmetric wavy channel. Fig. 4(a) and (b) show the streamwise u-velocity for laminar and periodic flow regimes, respectively, for an aspect ratio $r = 0.375$; whereas, Fig. 4(c) and (d), show pressure field and streamlines for the same laminar and time-periodic flow regimes, respectively. For laminar flow regimes, spatial periodicity in the velocity field develops in most of the extended computational domain, except in the first and last furrows, due to entrance and exit region effects. For time periodic flow regimes, spatial periodicity exists between furrows 3 and 7, as shown in Fig. 4(b). Entrance region effects do not allow the existence of periodicity in furrows 1 and 2; whereas, exit region effects do not allow the existence of spatial periodicity between furrows 8 and 12. The velocity field described in Fig. 4(b) corresponds to a time periodic flow, which continuously varies in time in the whole domain, but it holds spatial periodicity between furrows 3 and 7. Fig. 4(c) shows that for laminar flows the vortices in each furrow have the same strength along the channel and remain in the same relative position with respect to the inlet of each furrow between furrows 3 and 7. Last, Fig. 4(d) shows that for time periodic flows (despite the strong vortex dynamics that develops in each furrow), spatial periodicity holds between furrows 3 and 7. These numerical results are in very good agreement with numerical simulation results obtained by Guzman et al. [15,27,28] in symmetric wavy and grooved channels, Wang and Chen [20] and Vyas et al. [29].

3.2. Laminar and transitional flow regimes with a spatially periodic domain

This section presents numerical results obtained with the reduced domain models for laminar and transitional flow regimes, for the aspect ratios and Prandtl numbers of this investigation. The Reynolds number ranges are [40–300], [2–260], and [8–130], for the aspect ratios $r = 0.25$, 0.375, and 0.5, respectively. Fig. 5 shows streamlines for a Prandtl number of $Pr = 1.0$ and an aspect ratio $r = 0.375$. Fig. 5(a) shows streamlines for a laminar Reynolds number of $Re = 48$. The flow pattern is characterized by a parallel flow in the mid section, and two large and two small vortices, located at each furrow of the channel. In the mid channel section, between walls, the flow tends to follow the wavy shape of the channel shape, but it is constrained by the two large vortices. This flow pattern holds when the flow remains laminar and it changes first to a transitional periodic flow regime through a first Hopf bifurcation, and then, to a quasi-periodic flow regime through a second Hopf bifurcation. Fig. 5(b) shows a sequence of six instantaneous streamlines during one τ time period for a periodic transitional Reynolds number of $Re = 67$, and the same aspect ratio $r = 0.375$, and Prandtl number $Pr = 1.0$. This sequence demonstrates the wavy periodic nature of the flow as it moves downstream; it also shows a flow pattern of several vortices of different sizes,

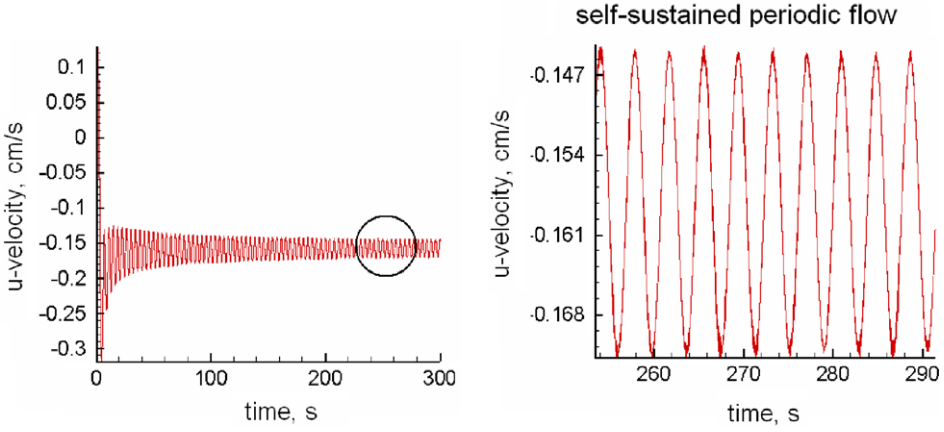

Fig. 3. Temporal evolution of u-velocity toward time periodic self-sustained flow regimes of $Re = 54.11$ for aspect ratio $r = 0.375$. Oscillatory nature of flow shown in close up of temporal evolution.

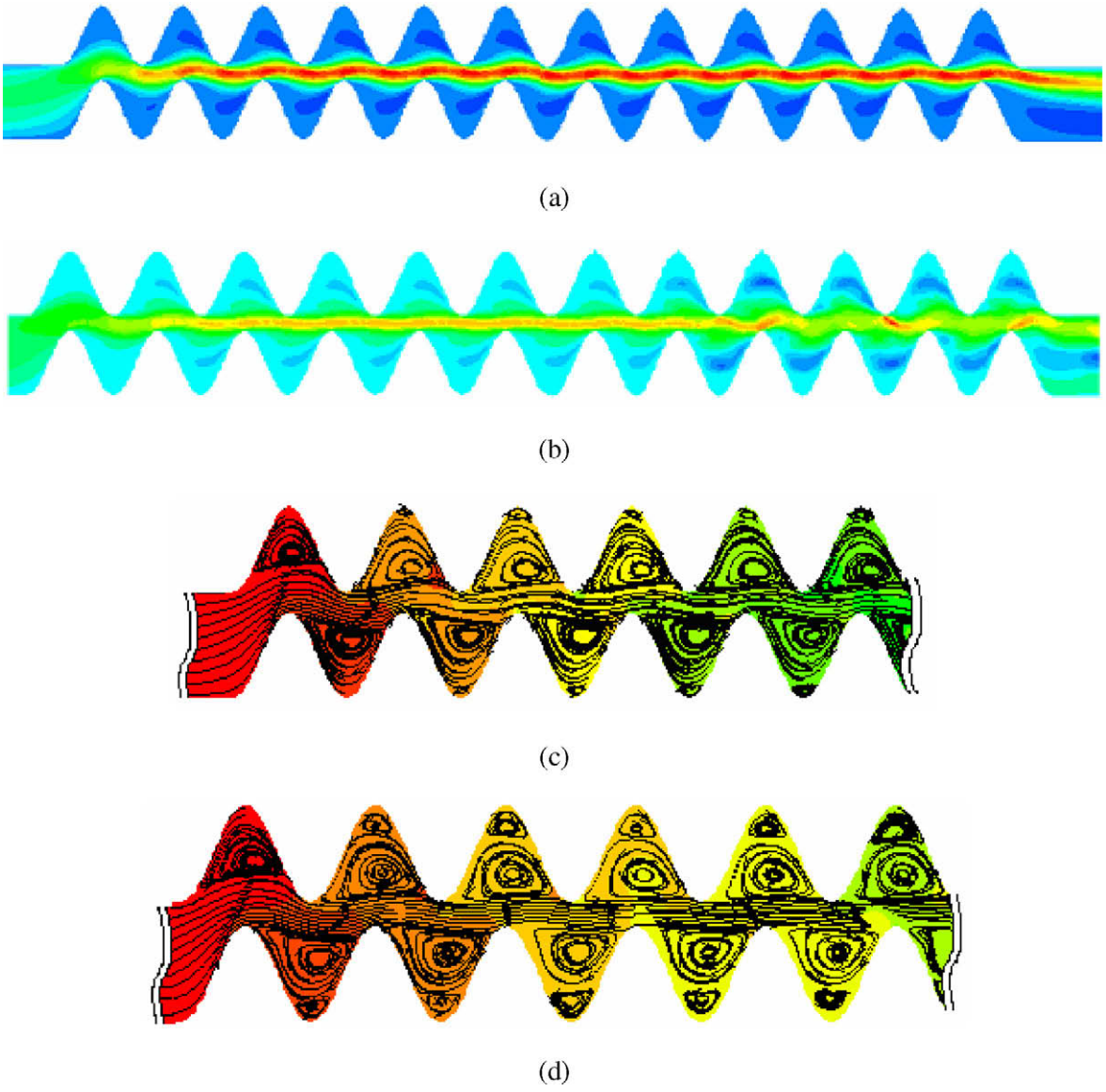

Fig. 4. Flow characteristics for extended domain: (a) u-velocity for laminar flow; (b) u-velocity for time-dependent flow regime; (c) pressure and streamlines for laminar flow; and, (d) instantaneous pressure and streamlines for time-dependent flow regime.

which increase and decrease in size as they are ejected from the wavy channel furrows. For higher transitional Reynolds numbers, the flow pattern preserves its wavy nature and shows a vortex dynamic that increases in intensity and strength and presents a wider variety of vortex sizes.

When the flow evolves to a periodic regime, the time periodic flow presents one fundamental frequency ω_1, and super-harmonics $2\omega_1$, $3\omega_1$, $4\omega_1,\ldots,n\omega_1$, with n, an integer number. The Eulerian flow characteristics of a quasi-periodic flow regime, in terms of temporal evolution of the u-velocity component, Fourier power spectrum and phase-portrait of the velocity components in a characteristic point of the computational domain for the aspect ratio $r = 0.375$, and Prandtl number $Pr = 1.0$, are presented in Fig. 6(a–c), respectively. This flow has evolved to a quasi- periodic flow regime from a periodic flow, through a second Hopf bifurcation at the critical Reynolds number, Rec_2 between $Re = 78.3$ and $Re = 79.8$. The Fourier power spectrum shows that the flow presents two fundamental frequencies, ω_1 and ω_2, and a linear combination of these frequencies, $n\omega_1 + m\omega_2$, where n and m are integers. The phase portrait depicts the quasi-periodic nature of this quasi-periodic flow, where a continuous shifting in the phase portrait representation develops because of the existence of the super harmonics $n\omega_1 + m\omega_2$.

In this asymmetric wavy channel, the transition scenario from a laminar to a time-dependent flow regime depends on the specific aspect ratio r. Fig. 7 shows a schematic representation of the transition scenarios for the three aspect ratios of this investigation. For an aspect ratio of $r = 0.375$, the transition scenario from a laminar to a quasi-periodic flow occurs by two successive Hopf bifurcations, B_1 and B_2 at Reynolds numbers Rec_1 and Rec_2, which are lower than the critical Reynolds number for a Poisueille plane channel flow. The transition scenario developed in this asymmetric wavy channel is very much like the Ruelle–Takens–Newhouse (RTN) scenario to chaos, developed in converging-diverging (symmetric wavy) channels and grooved channels, reported by Guzman et al. [15,24–26] and Wang and Chen [20]. The transition scenarios for the aspect ratios $r = 0.25$ and 0.5 are characterized by just one flow bifurcation to a time periodic flow. The critical Reynolds number of $Rec \approx 125$ for $r = 0.25$ is higher than the first critical Reynolds number of $Rec_1 \approx 54$ for $r = 0.375$, because for $r = 0.25$, the asymmetric

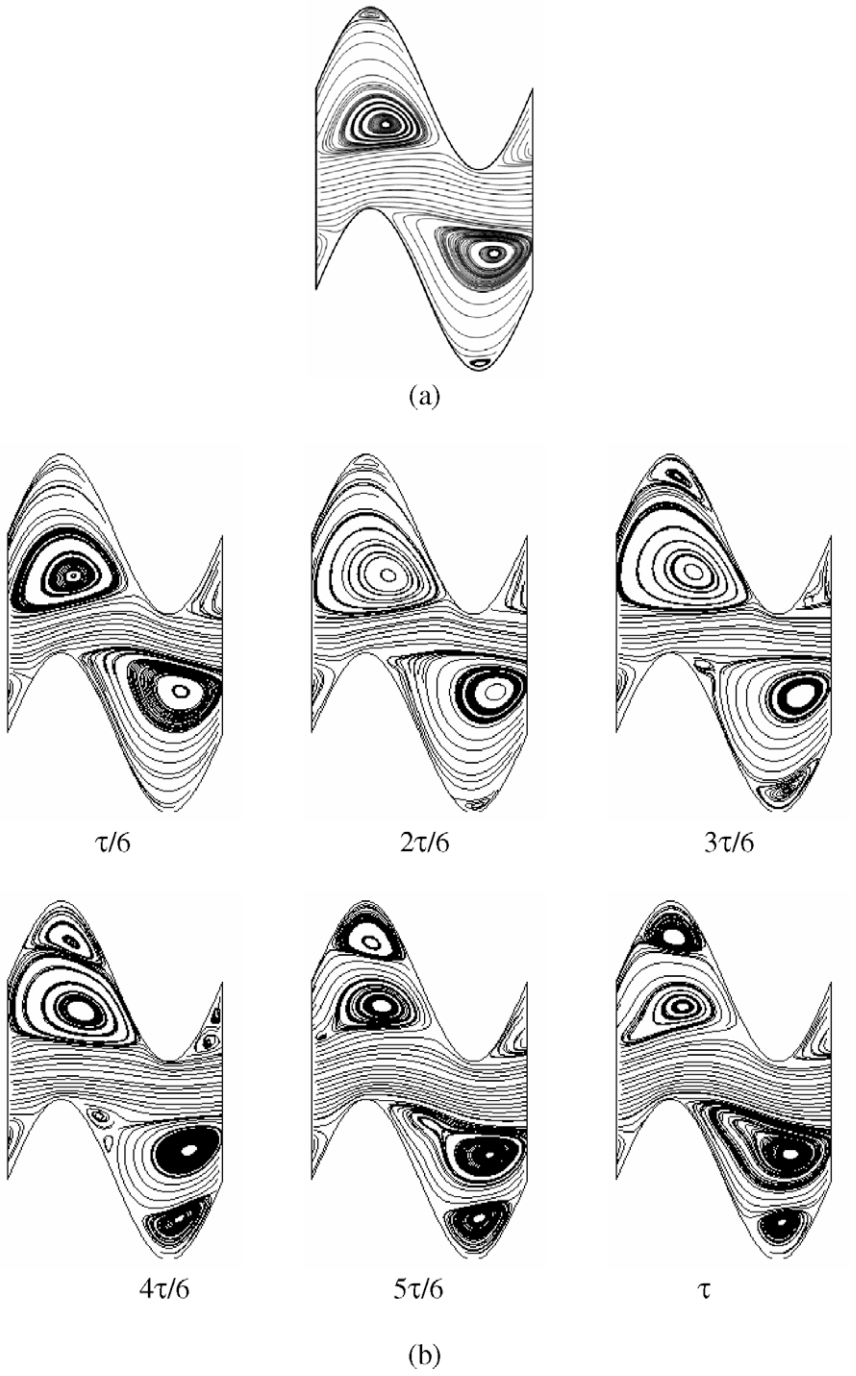

Fig. 5. Streamlines in reduced domain for aspect ratio $r = 0.375$ and $Pr = 1.0$: (a) laminar flow regime for Reynolds number of $Re = 48$; and, (b) six (6) instantaneous streamline representations during periodic transitional flow regime for Reynolds number of $Re = 67$.

wavy channel shape gets closer to the plane Poiseuille channel. The critical Reynolds number for $r = 0.5$ of $Rec_1 \approx 47$ is slightly smaller than the critical Reynolds number for $r = 0.375$, ($Rec_1 \approx 54$), because for $r = 0.5$, the asymmetric channel shape moves farther away from the Poiseuille plane channel shape. Thus, the flow easily looses stability because of the continuous change in direction of the flow as it moves downstream. For the aspect ratios of $r = 0.25$ and 0.5, further increases in the Reynolds numbers lead to a time periodic flow regime with higher fundamental frequency values, in the Reynolds number range of these simulations.

The flow characteristics for all the aspect ratios and Prandtl numbers have shown a flow dynamic during the transition scenarios that is characterized by high velocity and velocity gradients, which in turn generates high shear stresses, friction factors and pumping power requirements. Fig. 8 shows both the friction factor and pumping power as a function of the Reynolds number for the aspect ratios $r = 0.25$, 0.375 and 0.5, and for $Pr = 1.0$ and 9.4. Fig. 8(a) depicts the friction factor behavior for the asymmetric wavy channel and Poiseuille plane channel in the Reynolds number range of this investigation. The friction factor for the asymmetric wavy channel is calculated as $f_b = \frac{-\frac{dp}{dx}8h}{2\rho U^2}$, where $\frac{dp}{dx} = \frac{\Delta P}{L}$ is the fully developed pressure gradient in the streamwise direction; and L is the spatial periodic length. The Poiseuille plane channel friction factor is calculated as $f_p = 18/Re_H$, where Re_H is the Reynolds num-

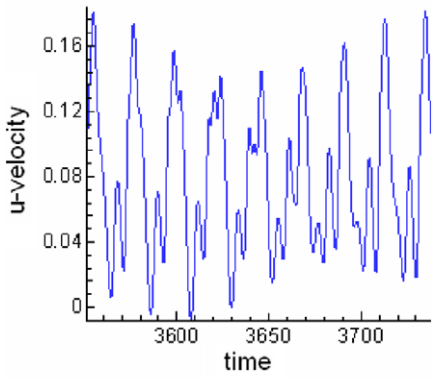

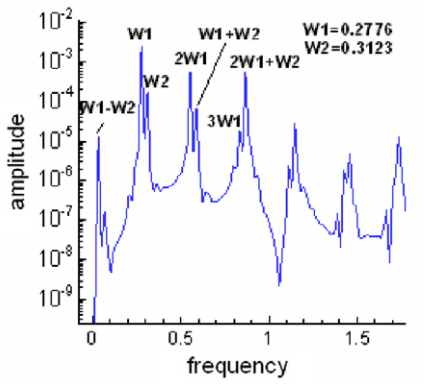

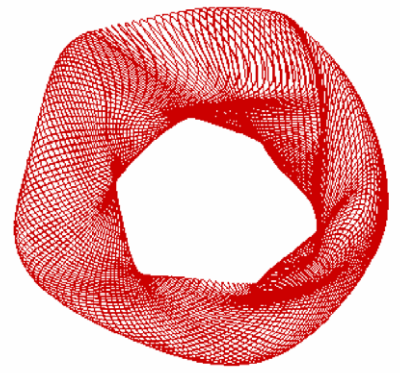

Fig. 6. Eulerian flow characteristics of quasi-periodic flow for Reynolds number of $Re = 84.62$, aspect ratio $r = 0.375$, and $Pr = 1.0$: (a) Temporal evolution of u-velocity; (b) Fourier power spectra of u-velocity; and, (c) phase-portrait of u- and v-velocity components.

ber, based on the height $H = 2\hat{h}$ of the plane channel. The friction factors for the three aspect ratios are higher than the friction factor for the Poiseuille plane channel for the entire Reynolds number range in this investigation. The highest friction factor develops for $r = 0.5$, which slightly increases as the Reynolds number increases; whereas, the lowest friction factor develops for $r = 0.25$, which continuously decreases with the Reynolds number increase. For the aspect ratio $r = 0.375$, the asymmetric wavy channel friction factor remains almost constant and is at least one order of magnitude higher than the Poiseuille plane channel friction factor. Fig. 8(b) shows the pumping power vs. Reynolds number for the three aspect ratios and two Prandtl numbers of these simulations. The pumping power continuously increases with the increase in

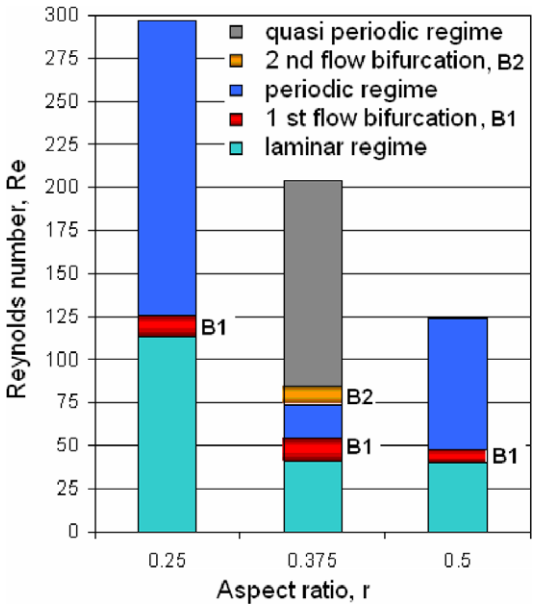

Fig. 7. Transition scenarios from laminar to a time-dependent flow by flow bifurcations for aspect ratios $r = 0.25$, 0.375, and 0.5. Two successive Hopf bifurcations, B_1 and B_2, for critical Reynolds numbers Rec_1 and Rec_2, respectively, develop for $r = 0.375$. Only one flow bifurcation from laminar to time periodic flow regime develops for aspect ratios $r = 0.25$ and 0.5.

the Reynolds number, regardless of the Prandtl number used in this investigation. For any given aspect ratio, and for a specific Reynolds number, the pumping power requirement is the same for both Prandtl numbers. The highest rate of pumping power increase occurs for $r = 0.5$; whereas the lowest rate occurs for $r = 0.25$. The pumping power requirements for $r = 0.375$ also increases with the Reynolds number increase, but its value remains between the pumping power requirements for $r = 0.25$ and 0.5, for any given Reynolds number in this investigation.

Laminar and transitional flows in asymmetric wavy channels demand a larger amount of energy to sustain them, in terms of pumping power, than is required in a plane channel flow. The flow must change direction continuously as it moves downstream through the waves in the channel. This demand increases as the flow evolves through a transition scenario due to the higher volumetric flow rate and the energy lost, associated with the higher Reynolds number and friction factor, respectively. The higher the aspect ratio, the higher is the demand on pumping power to push the flow through the successive asymmetric waves of the channel.

3.3. Heat transfer characteristics

The temperature distribution for laminar and transitional flow regimes for an aspect ratio $r = 0.375$, and Prandtl numbers $Pr = 9.4$ and 1.0, are shown in Figs. 9 and 10, respectively. Fig. 9(a) shows two stationary vortices and a thermal stratification for the laminar Reynolds number of $Re = 48$. The regions of high and low temperature remain steady in the lower and upper walls, respectively. During this laminar regime, the heat transfer process is dominated by a combination of convection and diffusion in the streamwise direction, and by diffusion in the crosswise direction. The large stationary vortices in each furrow of the asymmetric wavy channel prevent flow mixing and act as a thermal resistance to the transport of heat from the lower wall to the mean flow. Consequently, most of the heat concentrates near the lower wall and increases in temperature. Fig. 9(b) shows a sequence of six instantaneous representations of the temperature distribution in the asymmetric wavy channel during one time t period for a periodic

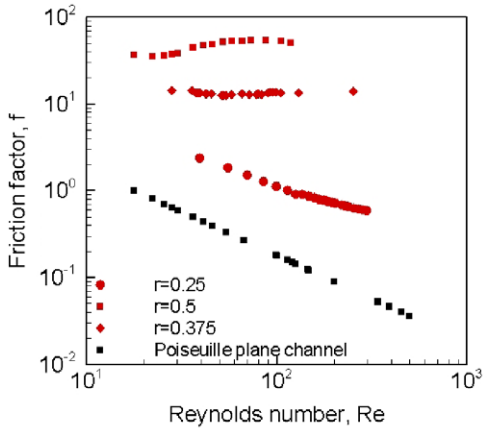

(a)

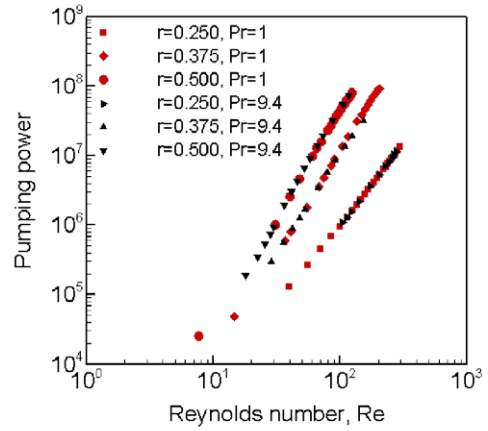

(b)

Fig. 8. Flow parameters for aspect ratios $r = 0.25$, 0.375, and 0.5, and Prandtl number $Pr = 1.0$ and 9.4: (a) friction factors vs Reynolds number for asymmetric wavy and Poiseuille plane channels; and (b) pumping power vs Reynolds number for asymmetric wavy channel.

flow regime of $Re = 78$. The temperature distribution presents several layers of time-dependent temperature stratification that resembles the wavy nature of this time periodic flow. The region of higher temperature is larger and closer to the mean flow region than in the laminar flow. Hotter fluid is ejected continuously from the hot lower surface to the mean flow; whereas colder fluid is pushed from the adiabatic upper wall to regions of higher temperature due to the improved flow mixing of this time periodic regime, which enhances the heat transfer rates.

Fig. 10(a) shows the streamlines and temperature distribution for the laminar Reynolds number of $Re = 36.83$. A pattern very similar to that of Fig. 9(a), with two stationary vortices, a thermal stratification, and steady regions of high and low temperature in the lower and upper walls, respectively, is observed. Because the heat transfer process is dominated by a combination of convection and diffusion in the streamwise direction, and there is very poor flow mixing, the thermal stratification pattern remains. Fig. 10(b) shows a sequence of five instantaneous representations of the temperature distribution during one time t period for a quasi-periodic flow regime of $Re = 182.36$. Although the several layers of time-dependent temperature stratification, which resemble the oscillatory nature of this quasi-periodic flow, remain; the temperature distribution presents regions where fluid zones of different temperatures combine and mix broadly. The mean flow region is more diffuse and less defined than the mean flow region of Fig. 9(b), with an interface that is less smooth. Hot fluid mixes continuously with colder fluid from both the mean flow and the upper wall region. In addition, colder fluid mixes better and flows toward the high temperature, lower wall region. This pattern, caused by the quasi-periodic flow, clearly enhances the convective mechanism of heat convection from the lower wall to the mean flow and upper wall regions.

Fig. 11 shows the heat transfer and flow parameters for laminar and transitional flow regimes for the aspect ratios $r = 0.25$, 0.375 and 0.5, and Prandtl numbers $Pr = 1.0$ and 9.4. Fig. 11(a) shows the time-average, mean Nusselt number as a function of the Reynolds number for laminar and transitional flow regimes. The time-averaged mean Nusselt number, or Nusselt number, is given by $Nu = \frac{\int_\tau \overline{Nu}(t)\cdot dt}{\int_\tau dt}$, where $\overline{Nu}(t)$ is the time-dependent mean Nusselt number calculated as $\overline{Nu}(t) = \frac{\int_L Nu(x,t)dx}{\int_L dx}$. Nu(x,t) is the local Nusselt number evaluated at the lower wall as $Nu(x,t) = \frac{q(x,t)\cdot \hat{h}}{k\cdot(T_w(x,t)-T_b(x,t))}$ and L is the integration length; $q(x,t)$ is the local heat flux along the wavy channel lower wall, $\hat{h}$ is the characteristic length, $T_w(x,t)$ is the lower wall temperature and T_b is the bulk temperature, defined as $T_b = \frac{\int_h^{\hat{h}} u(x_o,y,t)\cdot T(x_o,y,t)\cdot dy}{\int_h^{\hat{h}} u(x_o,y,t)\cdot dy}$ where x_o is the channel inlet. For a transitional flow regime, the time-dependent mean Nusselt number is integrated over a time period τ and normalized by the time period τ.

For all the aspect ratios and Prandtl numbers, the time-average mean Nusselt number increases with the Reynolds number as the flow evolves from a laminar to a transitional regime. For both Prandtl numbers, the highest increase in the Nusselt number, as the flow passes to the transitional regime, occurs for the aspect ratio $r = 0.5$; whereas, the lowest increases happens to $r = 0.25$. The increase of the Nusselt number for $r = 0.375$ is between $r = 0.5$ and $r = 0.25$. During the laminar regime, for the Prandtl number $Pr = 1$, the Nusselt number slightly increases in the range of $Nu = [2–4]$; whereas, for $Pr = 9.4$, the Nusselt number increase is in the range of $Nu = [3–5]$, regardless of the aspect ratio. An deformed circle in Fig. 11(a) indicates the region of small increase in the Nusselt number in the laminar regime. In the transitional regime, for a given aspect ratio and a given Reynolds number, the Nusselt number for $Pr = 9.4$ is much higher than for $Pr = 1.0$. For Prandtl number $Pr = 1.0$, increases of the Reynolds number in the transitional regime lead to a Nusselt number of about 6.3, 13.9, and 10.7, for the aspect ratios $r = 0.25$, 0.375 and 0.5, respectively. For Prandtl number $Pr = 9.4$, the Nusselt number reaches values of about 11.5, 26.9 and 28.8, for the aspect ratio $r = 0.25$, 0.375 and 0.5, respectively, as the Reynolds number is increased further in the transitional regime. That is, the Nusselt number for $Pr = 9.4$ is twice as much as for $Pr = 1.0$.

In the laminar regime, the increase in the Nusselt number is small because the heat transport from the lower wall to the mean flow is mainly due to a crosswise diffusion mechanism and a combination of streamwise convection and diffusion mechanism. As the flow evolves through the transitional flow regime, the higher Nusselt number is caused by flow mixing enhancement that develops in the periodic, and then the quasi-periodic, flow regimes. Both the momentum and heat fluxes are transported from the hot walls into the mean flow. The higher Nusselt number, obtained for $Pr = 9.4$ in the transitional regime, is caused by the higher value of the Peclet number $Pe = Re\cdot Pr$. For a given transitional Reynolds number, the higher the Prandtl number, the higher is the de Peclet number, and then the flow mixing enhancement and convective heat transfer mechanisms become more important. Thus, in transitional flow regimes, higher Nusselt numbers can be achieved when a higher Prandtl number fluid is used.

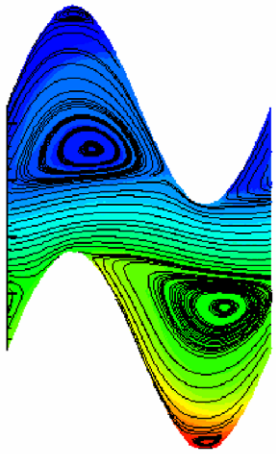

(a)

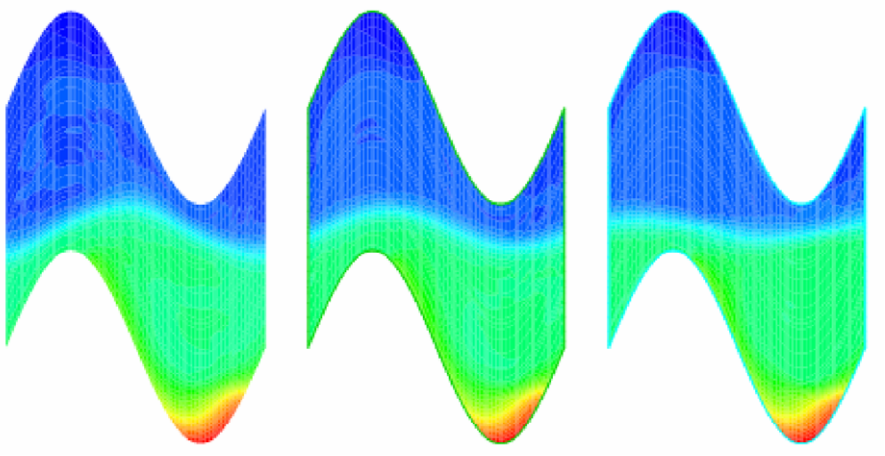

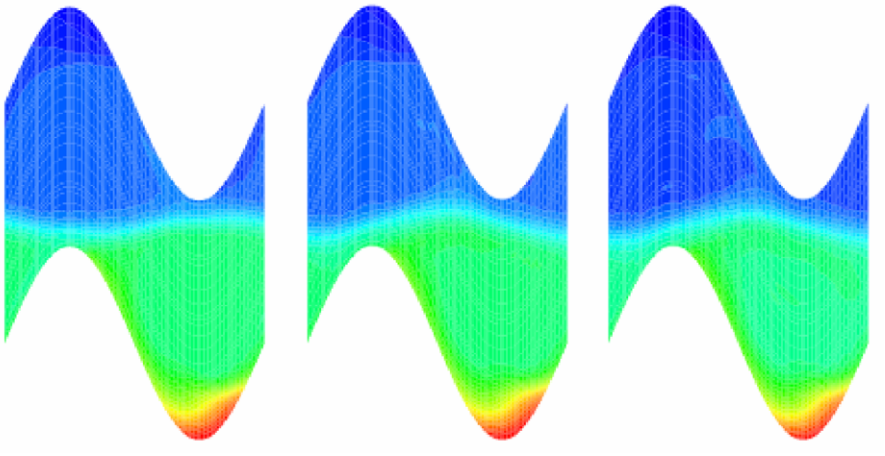

(b)

Fig. 9. Temperature distribution for $r = 0.375$ and $Pr = 9.4$: (a) laminar flow at $Re = 48$; and, (b) sequence of six (6) instantaneous representations for time periodic flow at $Re = 78$.

The increase of the Nusselt number – and therefore the heat transport enhancement – occurs at the expense of a higher value in the pumping power required for reaching the desired flow regimes. Fig. 11(b) shows the pumping power in terms of the Nusselt

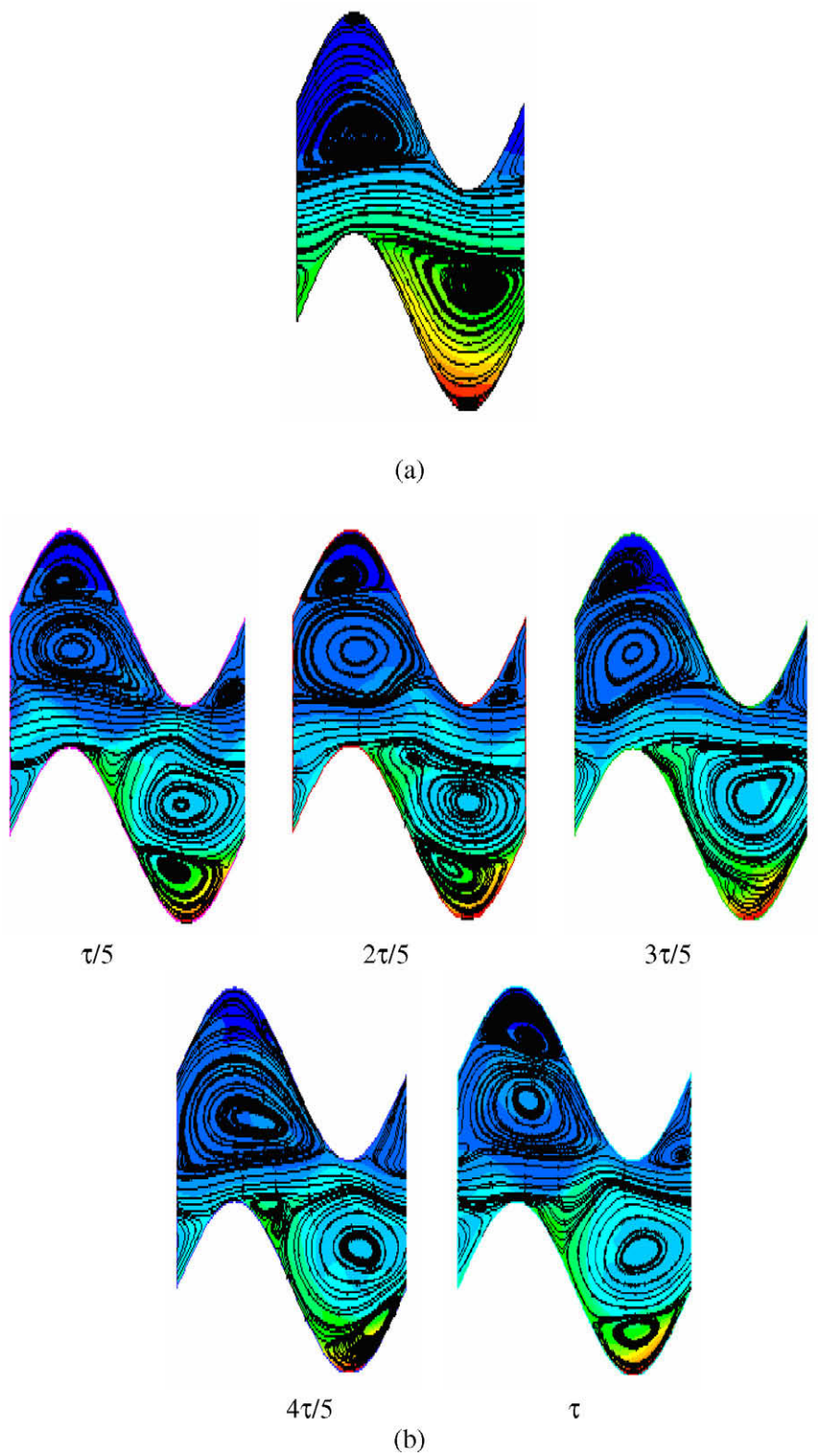

Fig. 10. Streamlines and temperature distribution for $r = 0.375$ and $Pr = 1.0$: (a) laminar flow at $Re = 36.83$; (b) quasi-periodic flow at $Re = 182.36$.

number for the aspect ratios $r = 0.25$, 0.375, and 0.5, and Prandtl numbers $Pr = 1.0$ and 9.4. As expected, for all the aspect ratios – and both Prandtl numbers – the demand for pumping power increases as the flow evolves through the transitional flow regime. For any of the Prandtl numbers of this investigation, the required amount of pumping power for reaching a specific Nusselt number grows as the aspect ratio increases from $r = 0.25$ to $r = 0.5$. This behavior is caused by the increased waviness of the wavy walls of the asymmetric channel for this aspect ratio; the flow must continuously change directions as it moves downstream, and therefore it demands more pumping energy to sustain a specific Reynolds number and heat transfer performance. In the laminar flow regime,

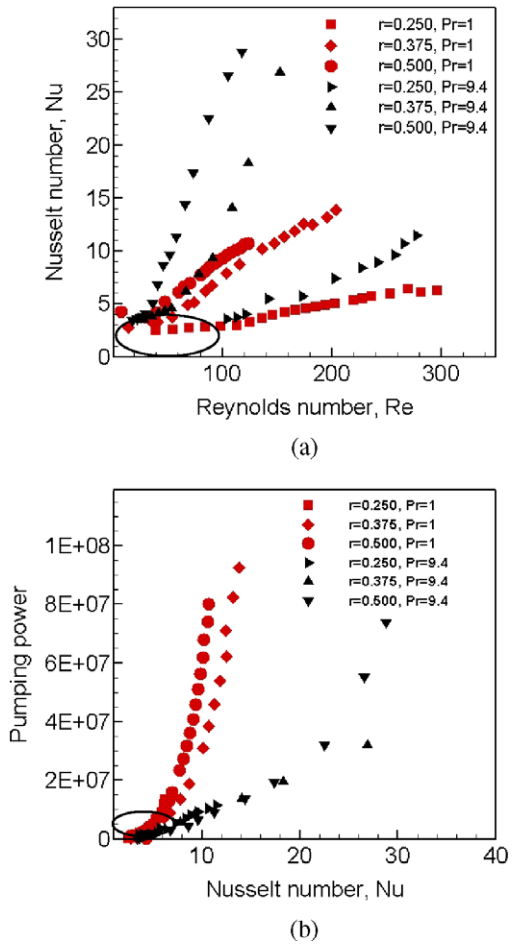

Fig. 11. Flow and heat transfer parameters for laminar and transitional flow regimes for aspect ratios $r = 0.25$, 0.375, and 0.5 and Prandtl numbers $Pr = 1.0$ and 9.4: (a) time-average mean Nusselt number vs. Reynolds number; (b) pumping power vs. time-average mean Nusselt number. In both figures laminar region indicated by a deformed circle.

the demand on pumping power is very moderate, as is the heat transfer performance. The pumping power demand for $Pr = 1.0$ for a given Nusselt number in the transitional regime is higher than the pumping power demand for $Pr = 9.4$, although higher Nusselt numbers are achieved for $Pr = 9.4$ than $Pr = 1.0$, as shown in Fig. 11(a). It is clear that $Pr = 9.4$ demands less pumping power and reaches higher Nusselt numbers than $Pr = 1.0$; although for $r = 0.5$, the pumping power demands for both Prandtl numbers are similar, but $Pr = 9.4$ leads to higher Nusselt numbers. For a given Prandtl number, higher Nusselt numbers can be obtained with higher aspect ratios, but higher pumping powers are required. Thus, in deciding what geometrical configuration and flow regime produce improved heat transfer performance, it is necessary to compromise the amount of heat transfer that can be obtained in a specific flow regime, and the cost of reaching that regime in terms of pumping power.

4. Summary and concluding remarks

The transition scenario in an asymmetric wavy channel, from laminar to time-dependent transitional flows, depends upon the channel aspect ratio r. Transition scenarios with one flow bifurcation develop for aspect ratio $r = 0.25$ and 0.5. For these two aspect ratios, the flow evolves from laminar to time-periodic flows, and further increases in the Reynolds number lead to periodic regimes. A scenario of two Hopf flow bifurcations develops for an aspect ratio $r = 0.375$, as the Reynolds number increases from a laminar to transitional regime. The first bifurcation at a $Re = Rec_1$ originates in a periodic flow characterized by one fundamental frequency ω_1. The second Hopf bifurcation at $Re = Rec_2 > Rec_1$, originates a quasi-periodic flow with two fundamental frequencies, ω_1 and ω_2, and linear combinations of these frequencies. For all the aspect ratios, the asymmetric wavy channel friction factors are higher than the Poiseuille plane channel friction factor, with the highest friction factor occurring for $r = 0.5$ and the lowest for $r = 0.25$.

For the laminar regime, the temperature distribution shows a pattern of stratification with the isotherms parallel to the streamlines; whereas in the transitional regime, the temperature distribution mimics the oscillatory wavy nature of the wavy walls and the periodic flows for $r = 0.25$, 0.375, and 0.5, and the quasi-periodic flows for $r = 0.375$. The vortex dynamics in the transitional regime enhances flow mix and improved the heat transfer process from the hot surfaces to the mean flow.

For all the aspect ratios and Prandtl numbers, the time-average mean Nusselt number – and consequently the heat transfer enhancement – increases with the Reynolds number as the flow evolves from a laminar to a transitional regime. For both Prandtl numbers, the highest increase in the Nusselt number, as the flow passes to the transitional regime, occurs for the aspect ratio $r = 0.5$; whereas the lowest increases occur to $r = 0.25$.

The increase of the Nusselt number, and therefore the heat transport enhancement, occurs at the expense of a higher value in the pumping power required to reach the desired flow regimes. For both Prandtl numbers in this investigation, the required amount of pumping power to reach a specific Nusselt number, grows as the aspect ratio increases from $r = 0.25$ to $r = 0.5$. This enhancement is obtained without the necessity for operating this channel to the high volumetric flow rates associated with turbulent flow regimes, which demand much greater pumping power. While no significant heat transfer enhancement is obtained for a laminar flow, significant heat transfer enhancement is obtained when the asymmetric wavy channel is operated in the appropriate transitional Reynolds number range.

Acknowledgements

The authors acknowledge the support of the research grant 1050087 of Fondecyt, the Fondo de Ciencia y Tecnología of Chile, and the Departmento de Ingeniería Mecánica at Universidad de Santiago de Chile.

References

[1] N.K. Ghaddar, K.Z. Korczak, B.B. Mikic, A.T. Patera, Numerical investigation of incompressible flow in grooved channels. Part 1. Stability and self-sustained oscillations, J. Fluid Mech. 163 (1986) 99–127.
[2] C.H. Amon, B.B. Mikic, Numerical prediction of convective heat transfer in self-sustained oscillatory flow, AIAA J. Thermophys. Heat Transfer 4 (1990) 239–246.
[3] M. Greiner, An experimental investigation of resonant heat transfer enhancement in grooved channels, Int. J. Heat Mass Transfer 34 (6) (1991) 1381–1391.
[4] M. Greiner, R.F. Chen, R.A. Wirtz, Augmented heat transfer in a recovery passage downstream from a grooved section: an example of uncoupled heat/momentum transport, ASME J. Heat Transfer 117 (2) (1995) 303–308.
[5] M. Greiner, M.R.J. Faulkner, V.T. Van, H.M. Tufo, P.F. Fischer, Simulations of three-dimensional flow and augmented heat transfer in a symmetrically grooved channel, ASME J. Heat Transfer 122 (4) (2000) 653–660.
[6] M. Greiner, P.F. Fischer, H.M. Tufo, Two-dimensional simulations of enhanced heat transfer in an intermittently grooved channel, ASME J. Heat Transfer 124 (3) (2002) 538–545.
[7] J.C.F. Pereira, J.M.M. Sousa, Finite volume calculations of self-sustained oscillations in a grooved channels, J. Comput. Phys 106 (1993) 19–29.
[8] B. Farhanieh, C. Herman, B. Sunden, Numerical and experimental analysis of laminar fluid flow and forced convection heat transfer in a grooved duct, Int. J. Heat Mass Transfer 36 (6) (1993) 1609–1617.

[9] J.S. Nigen, C.H. Amon, Time-dependent conjugate heat transfer characteristics of self-sustained oscillatory flows in a grooved channel, ASME J. Fluid Eng. 116 (3) (1994) 499–507.
[10] R.A. Wirtz, F. Huang, M. Greiner, Correlation of fully developed heat transfer and pressure drop in a symmetrically grooved channel, ASME J. Heat Transfer 121 (1) (1999) 236–239.
[11] T. Nishimura, K. Kunitsugu, A.M. Morega, Fluid mixing and mass transfer enhancement in grooved channels for pulsatile flow, J. Enhanced Heat Transfer 5 (1998) 23–27.
[12] T. Nishimura, N. Oka, Y. Yoshinaka, K. Kunitsugu, Influence of imposed oscillatory frequency on mass transfer enhancement of grooved channels for pulsatile flow, Int. J. Heat Mass Transfer 43 (13) (2000) 2365–2374.
[13] T. Adache, H. Uehara, Correlation between heat transfer and pressure drop in channels with periodically grooved parts, Int. J. Heat Mass Transfer 44 (22) (2001) 4333–4343.
[14] C. Herman, E. Kang, Heat transfer enhancement in a grooved channel with curved vanes, Int. J. Heat Mass Transfer 45 (18) (2002) 3741–3757.
[15] A.M. Guzmán, C.H. Amon, Transition to chaos in converging-diverging channel flows: Ruelle–Takens–Newhouse Scenario, Phys. Fluids A 6 (6) (1994) 1994–2002.
[16] A.M. Guzmán, C.H. Amon, Dynamical flow characterization of transitional and chaotic regimes in converging-diverging channels, J. Fluid Mech. 321 (1996) 25–57.
[17] A.M. Guzmán, C.H. Amon, Convective heat transfer and flow mixing in converging-diverging channel flows, in: Proceedings of the ASME Heat Transfer Division, vol. 1, HTD-Vol. 361-1, 1998, pp. 61–68.
[18] G. Wang, S.P. Vanka, Convective heat transfer en periodic wavy passages, Int. J. Heat Mass Transfer 38 (17) (1995) 3219–3230.
[19] G. Fabbri, Heat transfer optimization in corrugated wall channels, Int. J. Heat Mass Transfer 43 (23) (2000) 4299–4310.
[20] C.C. Wang, C.K. Chen, Forced convection in a wavy-wall channel, Int. J. Heat Mass Transfer 45 (12) (2002) 2587–2595.
[21] T. Nishimura, Oscillatory flow and mass transfer within asymmetric and symmetric channels with sinusoidal walls, Heat Mass Transfer 30 (1995) 269–278.
[22] A.T. Patera, A spectral element method for fluid dynamics: laminar flow in a channel expansion, J. Comput. Phys. 54 (3) (1984) 468–488.
[23] A. Ye, M. Shimizu, Augmented longitudinal diffusion in grooved tubes for oscillatory flow, Int. J. Heat Mass Transfer 44 (3) (2001) 633–644.
[24] M. Del Valle, A.M. Carrasco, A.M. Guzmán, Flow transitions and heat transfer in open block tandem channels, in: Proceedings of the ITherm 2002, International Conference on Thermal, Mechanics and Thermomechanical Phenomena in Electronic Systems, San Diego, California, 2002.
[25] M. Del Valle, Estudio y Análsis Mediante Simulaciones Computacionales de la Mecánica de Fluidos y Transferencia de Calor en Canales con Irregularidades Geométricas, Mech. Eng. Thesis, Universidad de Santiago de Chile, Santiago, Chile, 2001.
[26] P. E. Araya, Estudio y Análisis 2D del Flujo Laminar-Transicional y la Transferencia de Calor en un Canal de Paredes Sinusoidales Paralelas, Mech. Eng. Thesis, Universidad de Santiago de Chile, Santiago, Chile, 2001.
[27] F.A. Urzúa, Espectros de Fourier, Pseudo Espacio de Fase y Exponentes de Lyapounov en el Transporte e Fluido e Calor en Canales Sinusoidales Paralelos Asimetricos, Mech. Eng. Thesis, Universidad de Santiago de Chile, Santiago, Chile, 2005.
[28] M.J. Cárdenas, Mezclado de Flujo en un Canal de Paredes Sinusoidales Asimétricas Cerca de las Bifurcaciones del Flujo, Mech. Eng. Thesis, Universidad de Santiago de Chile, Santiago, Chile, 2006.
[29] S. Vyas, J. Zhang, R.M. Manglik, Steady recirculation and laminar forced convection in a sinusoidal wavy channel, ASME J. Heat Transfer 126 (4) (2004) 500.
[30] K.D. Stephanoff, I.J. Sobey, B.J. Bellhouse, On flow through furrowed channels. Part 2. Observed flow patterns, J. Fluid Mech. 96 (1980) 27–32.
[31] T. Nishimura, S. Matsune, Vortices and wall shear stresses in asymmetric and symmetric channels with sinusoidal wavy walls for pulsatile flow at low Reynolds numbers, Int. J. Heat Fluid Flow 19 (6) (1998) 583–593.